Research Article

Effects of Mass Loss on the Evolution of Wolf-Rayet Stars

Maria Volosatov[1]★

[1] *University of Victoria, Department of Physics and Astronomy, V8P, Canada*

27 April 2021

Abstract
Mass loss rates due to stellar winds in W-R stars for four simulations using the SYGMA (Stellar Yields for Galactic Modeling Applications)open source module are examined in this paper. The stellar properties predicted to have an effect on the mass loss rate of W-R stars, and consequently, their evolution along the W-R track. The depletion of layers can be modelled by the amount of ejecta per choice element, which are selected here to be helium, carbon, nitrogen, and oxygen. Higher metallicity and higher rotational velocity have been found to correspond with higher rates of mass loss.

1 Introduction

Wolf-Rayet stars (W-R stars) are massive, luminous stars with a unique spectrum featuring the agents of hydrogen-burning via the CNO cycle in the stellar interior. Occupying the upper-left region of the HR diagram, W-R stars are likely descendants of massive O and B-type stars with masses exceeding 40 $M_{\odot}$ (Abbott-Conti). They follow a classification scheme based on the elemental abundances of their spectra (WN stars featuring broad emission lines of helium and nitrogen, WC stars of carbon, oxygen and helium, and WO stars of O VI). The extreme luminosity of such stars and observation of W-R spectra leads us to postulate that radiation-driven mass loss contributes in large to the observed enrichment of the W-R's stars immediate environment by heavy metals, and to the evolution of W-R stars.

$$L_{Eddington} = 4\pi G m_p c/\sigma_T$$

Subject to strong interstellar winds, the hydrogen envelope has been stripped from W-R stars at earlier stages, as evident by the weak or absent hydrogen lines in the emission spectrum. Abbott et al. derive a mean mass-loss rate for W-R stars of $\dot{M} \approx 2\times10^{-5}$ (Abbott). The mass ejecta due to strong stellar winds should therefore be expected to show an abundance of heavier elements. The evolution of a SSP of W-R stars can be inferred analytically by gauging the isotopic abundances of their ejecta into the ISM. The goal of this paper is to analyze a SSP with the input of yields for massive stars from Limongi & Chieffi's paper(Limongi-Chieffi) using the SYGMA (Stellar Yields for Galactic Modeling Applications) module (Ritter et al.). In particular, I would like to examine (1) the amount in solar masses of the total and per isotope mass ejection (2) rates in $M_{\odot} yr^{-1}$ for a choice of eight isotopes, and (3) the effects of initial metallicity and equatorial rotation on the mass-loss rates of these stellar systems.

2 Methods

2.0.1 Creating Yield Tables

The yield tables were extracted from Table 30 of Limongi & Chieffi's data set of isotopic yields and converted into NuPyCEE yield tables using code provided in the publicly available code package at http://nugrid.github.io/NuPyCEE, the code for yield extraction generously provided by one of the authors, Côte(Ritter et al.). Each set includes masses [13, 15, 20, 25, 30, 40, 60, 80, 120] $M_{\odot}$ and metallicities [Fe/H] = 0, -1, -2, -3. Three yield tables were built for equatorial velocities v_{ini}= [0, 150, 300] km/s. The wind component with no contribution from SNe explosions was considered. The tables provide yields for 283 isotopic species ranging from H-1 to Bi-209.

2.1 Running the SYGMA Module

Following Limongi & Chieffi's summary on the constraints of mass for W-R stars, four data sets will be examined. The input parameters for the SYGMA module are described in Table 1.

a. **Non-rotating, solar-metallicity stars with initial masses 20-120** $M_{\odot}$ Their paper predicts that stars with initial mass exceeding 60$M_{\odot}$ at solar metallicity will lose substantial amounts of their hydrogen-rich envelope and become a WNL star.
b. **Non-rotating, sub-solar metallicity stars with initial masses 80-120** $M_{\odot}$ Stars with initial mass exceeding 60 $M_{\odot}$ at metallicities below $[Fe/H] = 0$ are expected to expand rapidly as central hydrogen is exhausted, however they never reach their Hayashi track due to substantial mass loss. At metallicities below $[Fe/H] = -2$ ($Z < 10^{-3}$) no W-R stars are expected.
c. **Rotating (v_{ini} = 150 km/s), sub-solar metallicity stars with initial masses 20-120** $M_{\odot}$ Mass loss is strongly enhanced for rotating models as it pushes stars above their Eddington luminosity limit at the end of their hydrogen burning stage. Beyond helium burning, rotation is not predicted to have a significant impact on the evolution of such stars.
d. **Rotating (vini = 300 km/s), sub-solar metallicity stars with initial masses 20-120** $M_{\odot}$ See (c). This set is to gauge the scale on which rotation speed impacts mass loss rates.

The time evolution of accumulated mass ejecta was plotted for each model. Where mass parameters needed to be constrained, there are two runs, one with the full range of masses available (1-120) and another covering the lower limit. The cumulated mass ejecta for massive stars as a function of time was extracted for each time step in the simulation. SYGMA provides functions for the retrieval of needed values, such as the his-

Table 1. SYGMA input parameters

Simulation	z	M_{gas}	M_{tran}	IMF range	IMF Type
1	0.02	1.0	8.0	20-120	Salpeter
2	0.002	1.0	8.0	80-120	Salpeter
3	0.002	1.0	8.0	1-120	Salpeter
4	0.002	1.0	8.0	1-120	Salpeter

SYGMA input parameters for four runs. M_{gas} is the initial mass of gas content which has been kept at 1.0 $M_{\odot}$ to scale the mass ejecta. M_{tran} is the initial mass which marks the transition from AGB to massive stars. The IMF range is not the exact format of the input parameters, the subtraction to achieve these desired ranges is explained.

Table 2. Simulation 1

Element	Time (10^6 years)	Mass ejected$M_{\odot}$
All	9.84	0.054
He	9.84	0.024
C	9.84	4.0 $\times 10^{-4}$
N	9.84	2.2 $\times 10^{-4}$
O	9.84	2.1$\times 10^{-4}$

Non-rotating, 20-120$M_{\odot}$ at z=0.02

tory.age which is the time against which the cumulated ejecta is plotted. Running the code to extract the cumulated ejecta for massive stars allowed for the subtraction of ejecta of the lower mass limit run from the full mass range run, cutting off the contributions from stars beneath the upper limit for the lower mass limit run. The resulting plots show the difference. The process was repeated for the second data set (no rotation, subsolar metallicity) subtracting the 1-120 run from the 1-60 and the 1-80 run to get the cumulated ejecta as a function of time (plotted as the difference) for masses 60-120 and 80-120 at subsolar metallicity. Note that this includes all elements, however the same procedure was used to extract the accumulated mass ejecta for helium, carbon, nitrogen, and oxygen. No subtraction to constrain masses was needed for the difference plots of the rotating models. The comparison to see the effects of rotation on mass loss was between 0 km/s, 150 km/s, and 300 km/s, all runs with IMF constraint 1-120 $M_{\odot}$ at subsolar metallicity. The mass loss rate for specific isotopes was plotted for several species against the time steps. The isotopic mass loss rates for different parameters (differing metallicities or rotational velocities) were plotted to show the difference in mass loss rates at each time step.

3 Results

3.1 SSP at solar metallicity, no rotation

The ejecta of a population of non-rotating, solar metallicity stars between ranges 1-120$M_{\odot}$ and 1-20$M_{\odot}$ are plotted showing the contribution of all sources (AGB, Massive, and SNe) and only the massive sources (Appendix A, figures 1.1,1.2). There is an increase in the amount of mass ejected with time as stars evolve and more stars eject matter. The plateau observed most prominently in the ejected mass of massive stars indicates that at some time step, no more mass is ejected due to winds—evidently the star has evolved off of its nuclear timescale and considering the short lifetime of such stars, ended as a supernova. Since contributions from supernovae are not included, the mass ejected flattens out to a constant value.

After subtracting the two runs to achieve the difference for the desired mass range, the evolution of the cumulated mass ejecta is plotted in green (Appendix A, fig. 1.3). The point before the curve flattens out is found via interpolation to be at 9840582.55 $\approx$ 9.84 $\times 10^6$ years, at which point 0.054 $M_{\odot}$ of material has been blown off. Although there is evidently no strict linear relation, the mass ejecta after this period of time will be used in comparison with the following runs to show which stellar parameters affect the rate of mass loss the most. The difference is also plotted for the accumulated mass ejecta for helium, carbon, nitrogen, and oxygen. While it is possible to obtain the accumulated mass ejecta for heavier elements, the abundances are notably lower and the four elemental species described can be considered the indicators for which evolutionary stage a W-R star is at (recall that spectra of W-R stars show an abundance of whichever interior material is currently exposed).

Table 3. Simulation 2

Element	Time (10^6 years)	Mass ejected$M_{\odot}$
All	3.69	0.0054
He	3.69	0.0024
C	3.69	3.47 $\times 10^{-6}$
N	3.69	5.04 $\times 10^{-6}$
O	3.69	6.40 $\times 10^{-6}$

Non-rotating, 80-120$M_{\odot}$ at z=0.002

3.2 SSP at subsolar metallicity, no rotation

The ejecta of a population of non-rotating subsolar metallicity stars for three mass ranges rather than two has been plotted as 80-120 was too narrow a mass range to determine with confidence whether a lower metallicity results in more or less rapid mass loss. Performing a subtraction of the runs as before we get two differences (Appendix B, fig. 2.3). The differences for the four elements of interest have been plotted (Appendix B, fig. 2.4-2.7). We see that the plateau is reached at an earlier time step for subsolar metallicity, suggesting that mass loss terminates sooner, however only 10 $\%$ of the mass amount ejected under solar metallicity conditions is ejected in a factor of 0.4 the time at subsolar metallicity. This leads to the assumption that wind-driven mass loss is less rapid for lower metallicities and ceases to contribute to the ejecta at an earlier time. Notable is also the fact that heavier element abundances, particularly after and including carbon, are significantly lower at the plateau.

3.3 SSPs with rotational velocities 150 km/s and 300 km/s

The mass ejecta of three populations are plotted at varying equatorial rotations, each at z=0.002, with masses ranging 1-120$M_{\odot}$ to examine the effects of rotation on mass loss rates. It is evident from fig. 3.2 (Appendix C) that the addition of equatorial velocity increases the mass loss rate. For 150 km/s, the amount of mass ejected over a time period of 36 $\times 10^6$ is greater than the mass ejected for 0 km/s velocity by a factor of 2. Increasing the equatorial velocity further does not significantly increase the amount of mass lost: for an equal time period, 0.052 $M_{\odot}$ is ejected at v=300 km/s. It is expected that at greater rotational velocities, the surface abundance of heavy elements should increase as the interior products of fusion are mixed and brought up to the surface.

Table 4. Simulation 3

Element	Time (10^6 years)	Mass ejected$M_\odot$
All	36	0.048
He	36	0.019
C	36	4.0 $\times 10^{-4}$
N	36	4.98 $\times 10^{-5}$
O	36	1.1 $\times 10^{-4}$

v_{rot}=150km/s 1-120$M_\odot$ at z=0.002

Table 5. Simulation 4

Element	Time (10^6 years)	Mass ejected$M_\odot$
All	36	0.053
He	36	0.023
C	36	5.0 $\times 10^{-4}$
N	36	8.5 $\times 10^{-5}$
O	36	1.4 $\times 10^{-4}$

v_{rot}=300km/s 1-120$M_\odot$ at z=0.002

4 Discussion

We see that from simulation 1 and 2, the mass loss rate is higher at solar metallicity than it is for subsolar. Finding the difference for the subsolar metallicity model for mass ranges 60-120 and 80-120 shows that, while the ejected mass approaches a constant value 6.15 $\times 10^6$ years earlier than in simulation 1, the mass ejection values for all elements are 10 $\%$ the amount ejected for all elements in the solar metallicity model. The same trend is repeated for helium, however the solar model ejecta shows carbon ejection exceeds the subsolar model by a factor of 115, nitrogen by a factor of 43, and oxygen by a factor of 32. Even when examined at the same time step as the solar model, the subsolar model shows a consistent lower mass loss rate. If we assume the evolutionary trend of W-R stars transition them between WN, WC, and WO types, and a sequential evolutionary track holds (WC evolve from WN, WO evolve from WC), it can be inferred that higher rates of depletion of a particular element predicted to have a relatively high surface abundance for a given star corresponds to a more rapid rate of evolution along the sequence of the W-R phase. In the case of metallicity, higher metallicity appears to correspond with higher mass loss rates, which leads to more rapid loss of the star's outer layers, so a star can be expected to lose helium more rapidly and show a WC spectrum. Examining the plots showing the evolution of mass loss rate for the 4 elements of choice (Appendix D, fig. 4.1-4.4), there is distinct fluctuations in the slopes between time steps for both models, but overall there is a downward trend in mass loss rate, suggesting the highest mass loss rate occurs at time-step 2.66 $\times 10^6$ years, and progressively slows down with the depletion of the choice element.

Simulations 3 and 4 show the distinct effect of rotational velocity on the mass loss rates. Introducing 150 km/s rotational velocity dramatically increases the amount of mass ejected for an SSP at the same metallicity as the non-rotational model. Likely due to the IMF range and metallicity choice, the time to reach a plateau is notably much longer than the previous two simulations. The mass ejected for the non-rotational model reaches a constant value of 0.023 solar masses at 36 $\times 10^6$ years, while the v=150km/s model reaches 0.048 in the same amount of time—over 2 times the amount of ejecta than the non-rotational model. This relation appears to converge as we double the rotational velocity again to 300 km/s, but the mass ejecta is only 2.3 times that of the non-rotational model. Comparing the two non-zero rotational velocity models, simulation 4 ejects 1.2 times the amount of helium as simulation 3, 1.25 times the amount of carbon, 1.7 times the amount of nitrogen, and 1.3 times the amount of oxygen. The effects of rotation influence mass loss more prominently at subsolar metallicity, and it is expected that with greater rotation rates, mixing of interior nuclear-burning products will be more pronounced, and surface abundance of heavier elements enhanced, which as predicted for the solar metallicity model, corresponds to higher rates of mass loss. Three models are plotted for each rotational velocity examining the four elements of choice. Helium mass loss progresses steadily downwards with the non-rotational model, while the two non-zero rotational models follow closely (Appendix C, fig. 3.4). There is a greater difference in the accumulated mass ejecta of carbon (Appendix C. fig. 3.5) than in other elements, implying that a greater amount of carbon is ejected in the rotating models. This may indicate that the carbon layer is depleted by stellar winds at such a rate that the star evolves faster off the WN-WC track.

If we assume that more rapid rates of mass loss progress a star along its evolutionary track for W-R stars, rotational velocity has a greater impact on the mass loss rate than metallicity, and higher metallicity corresponds to higher mass loss rates.

5 Conclusion

By examining the mass loss rates for 4 simulations, the first pair examining the effects of metallicity on mass loss rates and the second pair examining the effects of rotational velocity, it was determined that higher metallicity and higher rotational velocity are linked to higher mass loss rates. The integrated mass of the ejecta in each simulation was determined for each of the 4 simulations as the point before the plateau seen in the mass of the ejecta for all elements plots: 0.054 $M_\odot$ for solar metallicity, 0.0054 $M_\odot$ for subsolar metallicity, 0.048 $M_\odot$ for a rotational velocity of 150 km/s, and 0.053 $M_\odot$ for a rotational velocity of 300 km/s.

The rates per isotope plots provided in Appendix D for simulations 1 and 2 and Appendix E for simulations 3 and 4 in $M_\odot\ yr^{-1}$ show a downward trend in the rate with time evolution, however a linear fit seemed a hasty assumption which would require a more detailed examination before being deemed appropriate to apply.

The SYGMA module provided an excellent opportunity to study mass loss rates in W-R stars, with the addition of Limongi and Chieffi's yield tables. Further work could benefit from employing the OMEGA module to study an existing W-R star rich environment, such as the Sculptor dwarf galaxy.

Please see the list of references after Appendix E.

Software: SYGMA (Ritter et al. (2017), NuPyCEE (Ritter Côté 2016), Cyberhubs (Herwig et al. 2018), NumPy (Van Der Walt et al. 2011), matplotlib (https://matplotlib.org).

6 Appendix A

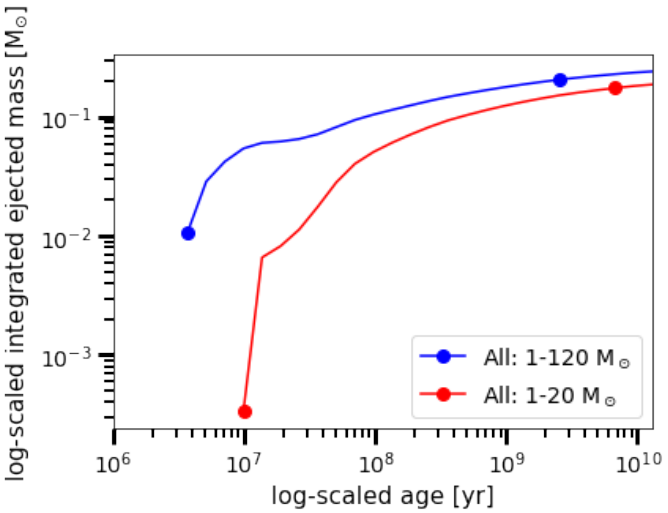

Fig. 1.1 Mass ejected for all sources for simulation 1

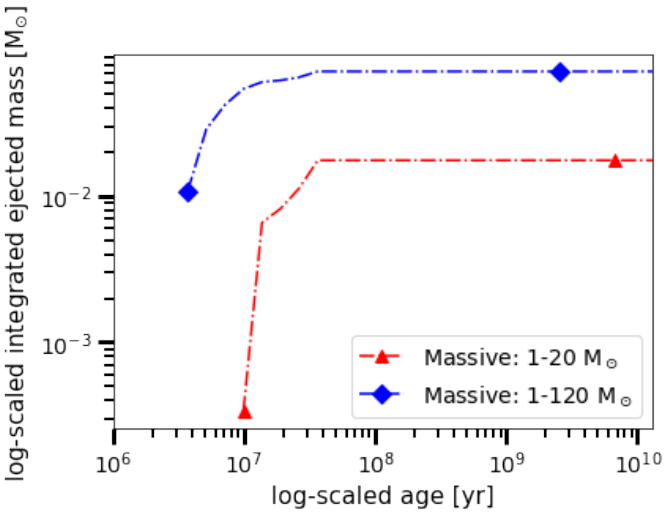

Fig. 1.2 Mass ejected for massive stars for simulation 1

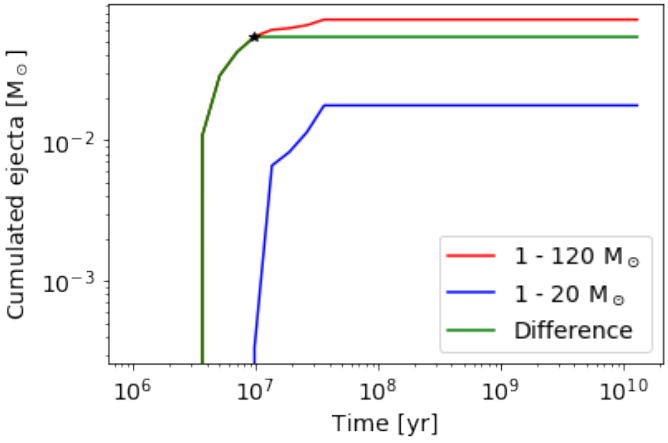

Fig. 1.3 Mass ejected for massive stars for simulation 1 with difference

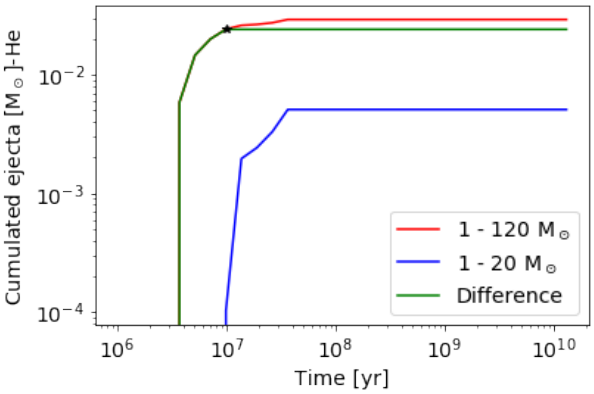

Fig. 1.4 Helium Mass ejected for simulation 1

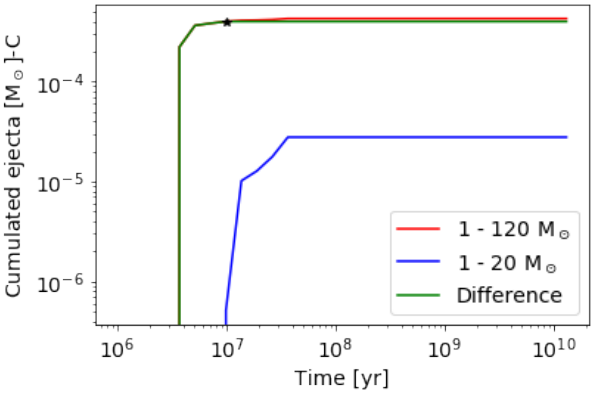

Fig. 1.5 Carbon Mass ejected for simulation 1

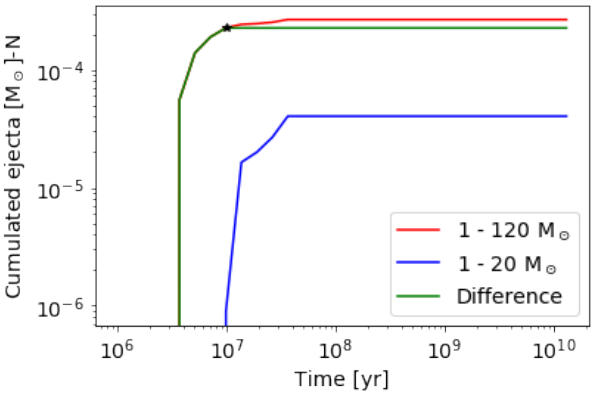

Fig. 1.6 Nitrogen Mass ejected for simulation 1

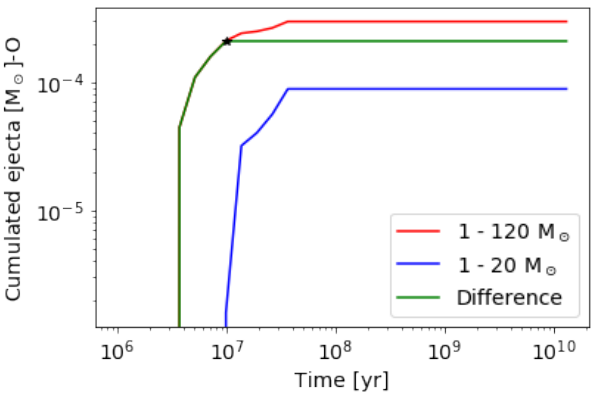

Fig. 1.7 Oxygen Mass ejected for simulation 1

7 Appendix B

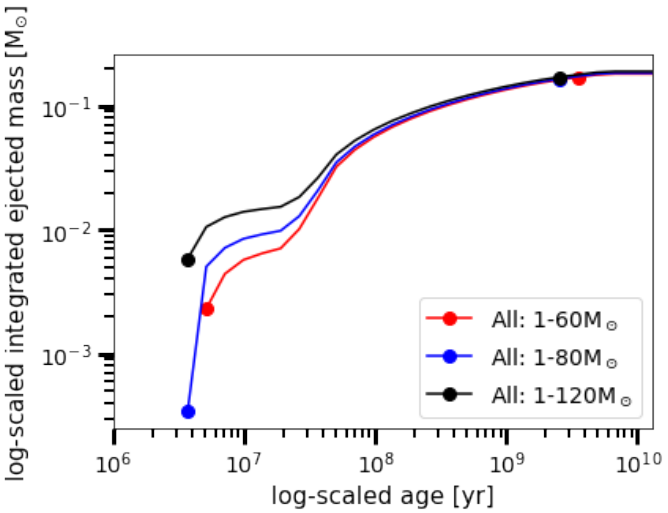

Fig. 2.1 Mass ejected for all sources for simulation 2

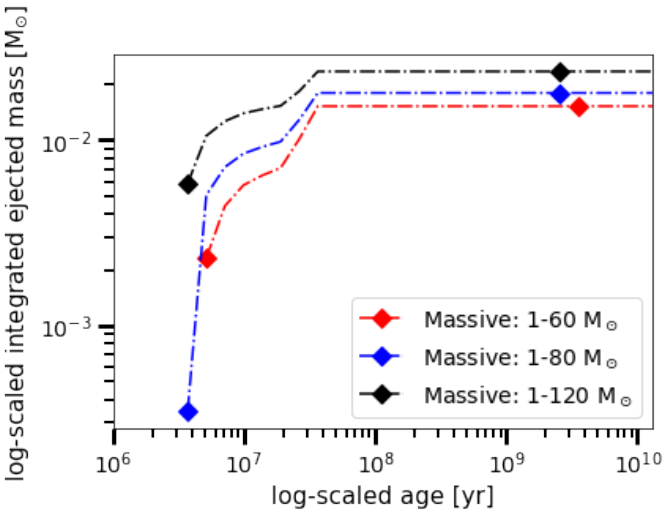

Fig. 2.2 Mass ejected for massive stars for simulation 2

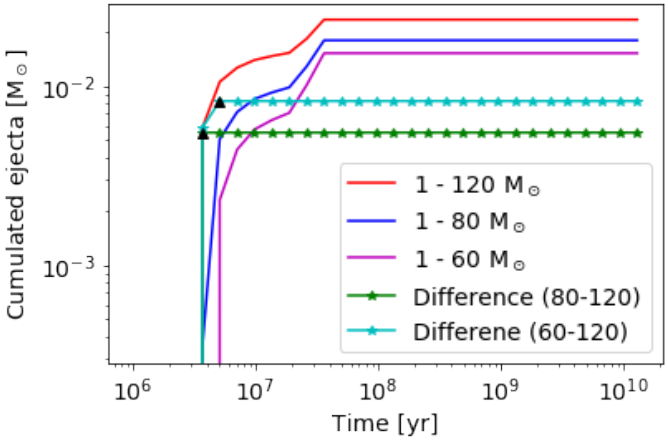

Fig. 2.3 Mass ejected for massive stars for simulation 2 with difference

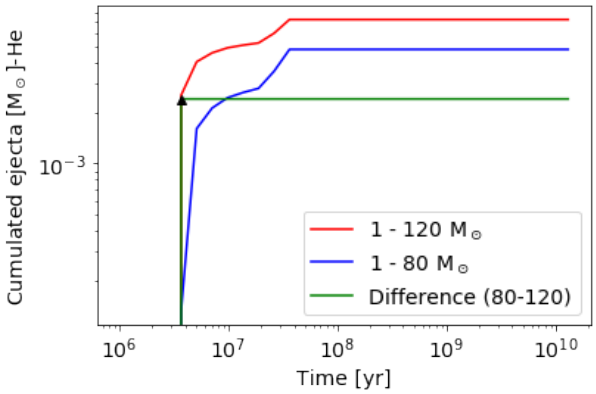

Fig. 2.4 Helium Mass ejected for simulation 2

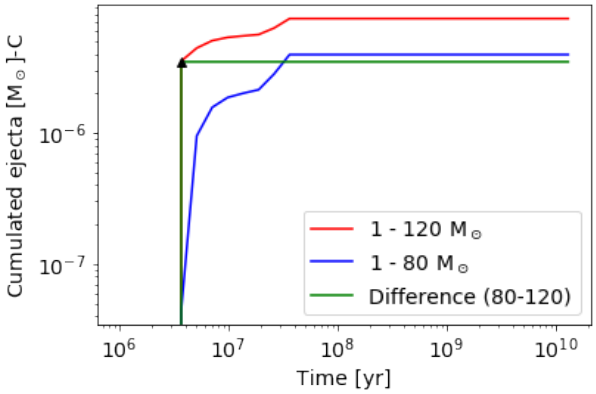

Fig. 2.5 Carbon Mass ejected for simulation 2

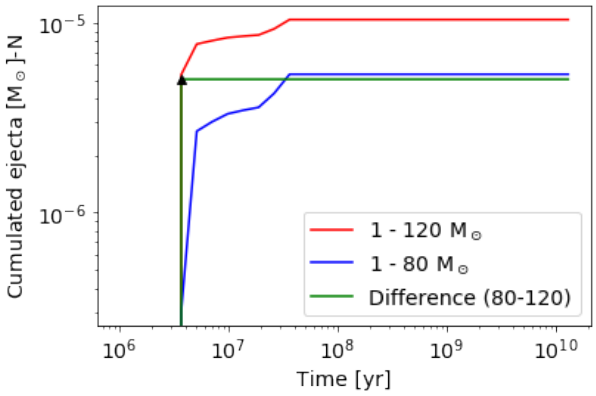

Fig. 2.6 Nitrogen Mass ejected for simulation 2

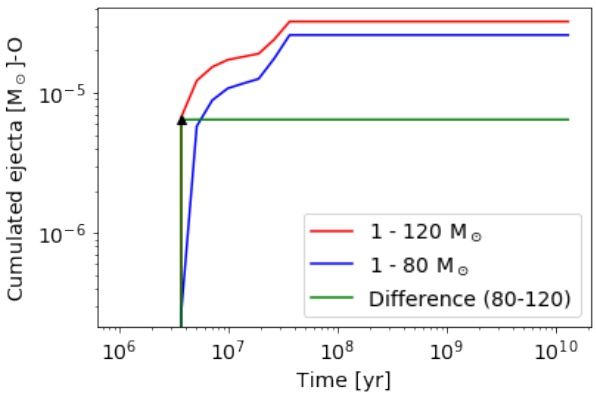

Fig. 2.7 Oxygen Mass ejected for simulation 2

8 Appendix C

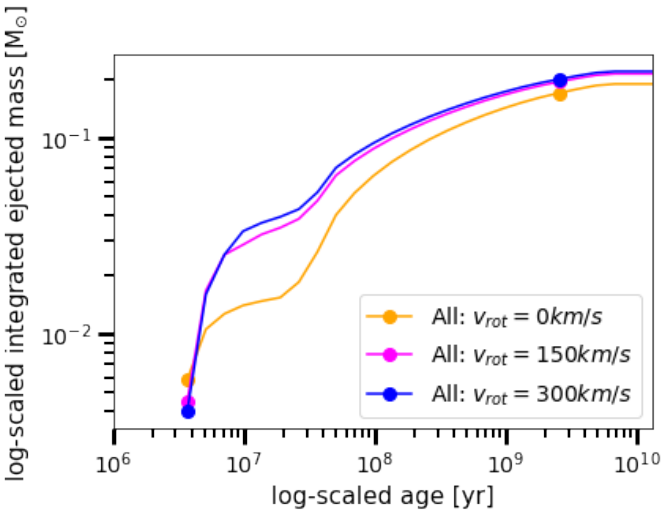

Fig. 3.1 Mass ejected for all sources for simulations 3,4

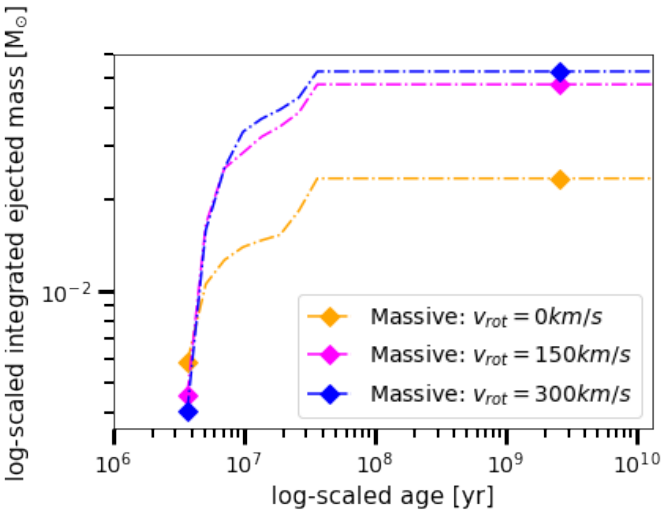

Fig. 3.2 Mass ejected for massive stars for simulations 3,4

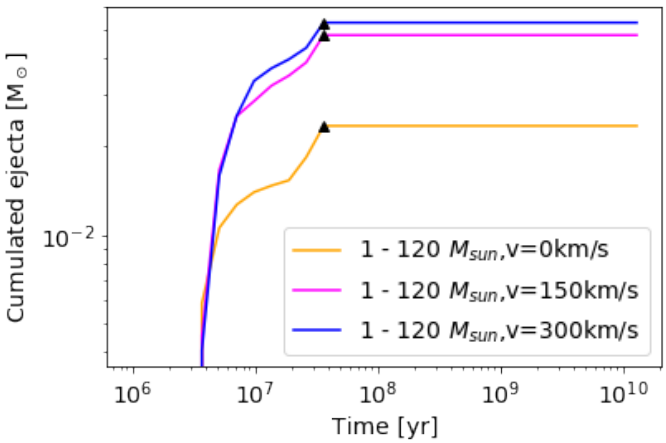

Fig. 3.3 Mass ejected for massive stars for simulation 3,4 and against 0 km/s rotational velocity

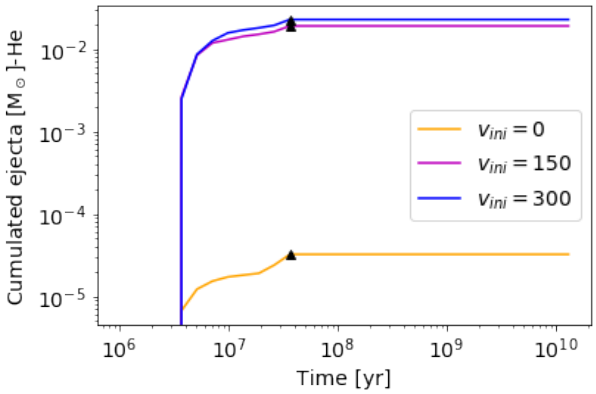

Fig. 3.4 Helium Mass ejected for simulations 3,4

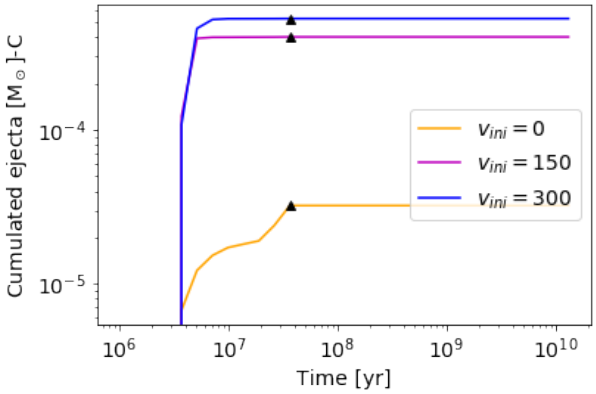

Fig. 3.5 Carbon Mass ejected for simulations 3,4

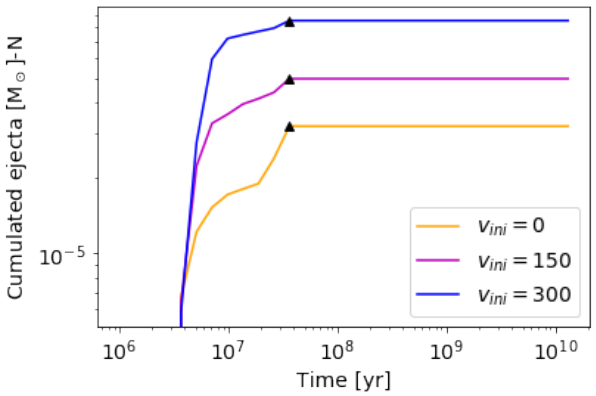

Fig. 3.6 Nitrogen Mass ejected for simulations 3,4

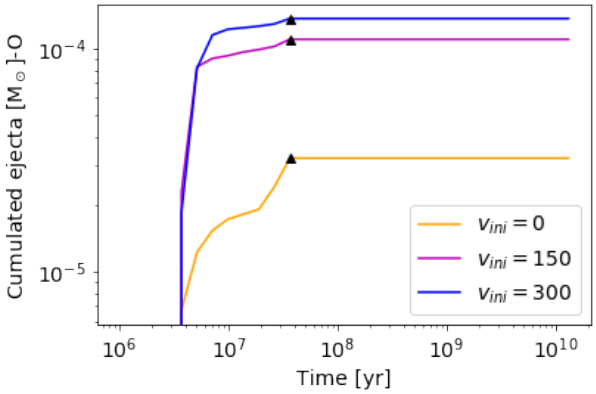

Fig. 3.7 Oxygen Mass ejected for simulations 3,4

9 Appendix D

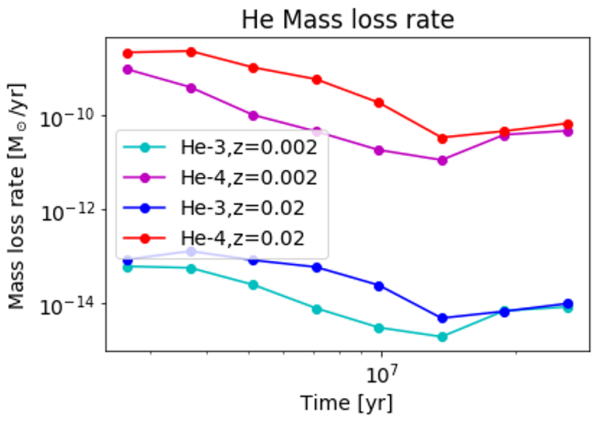

Fig. 4.1 Helium mass-loss rate for simulations 1,2

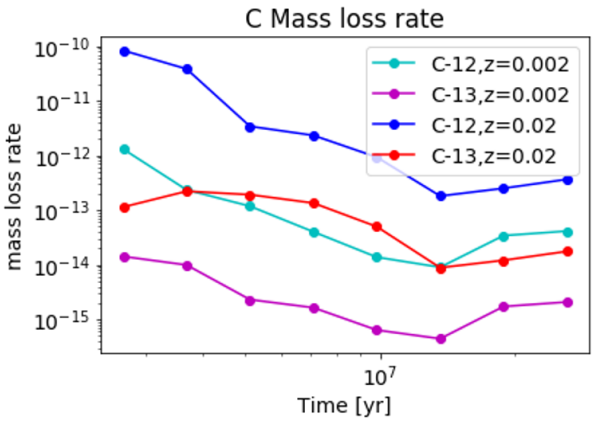

Fig. 4.2 Carbon mass-loss rate for simulations 1,2

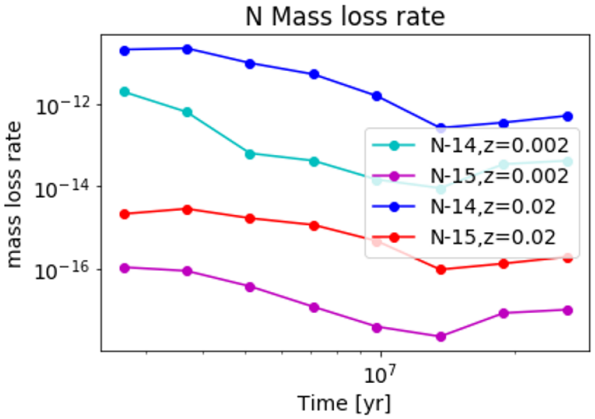

Fig. 4.3 Nitrogen mass-loss rate for simulations 1,2

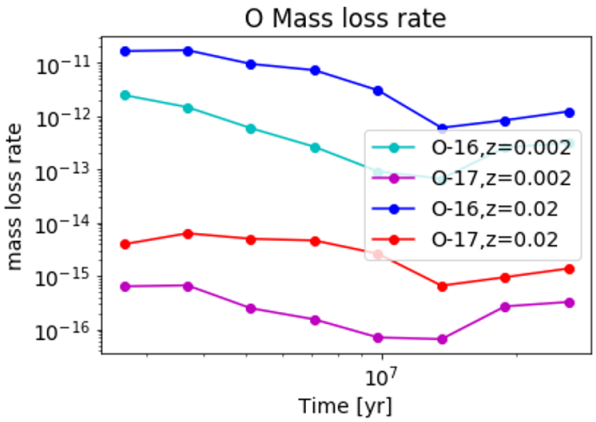

Fig. 4.4 Oxygen mass-loss rate for simulations 1,2

10 Appendix E

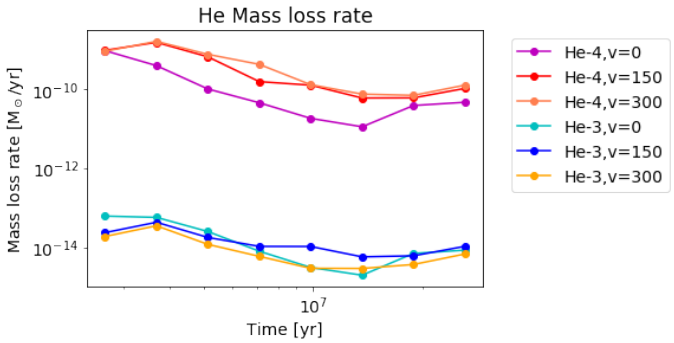

Fig. 5.1 He mass-loss rate for simulations 3,4

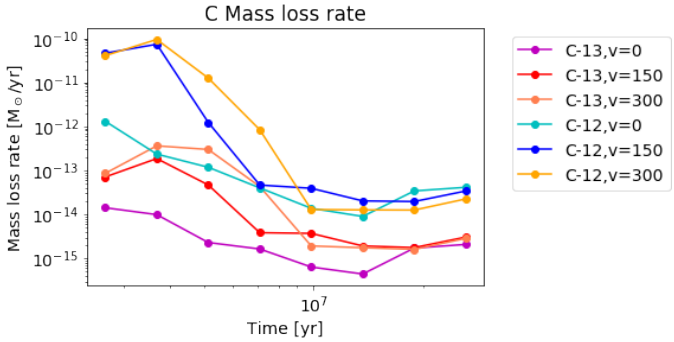

Fig. 5.2 C mass-loss rate for simulations 3,4

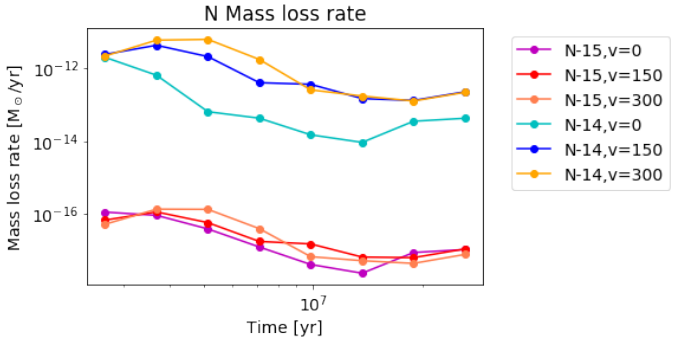

Fig. 5.3 N mass-loss rate for simulations 3,4

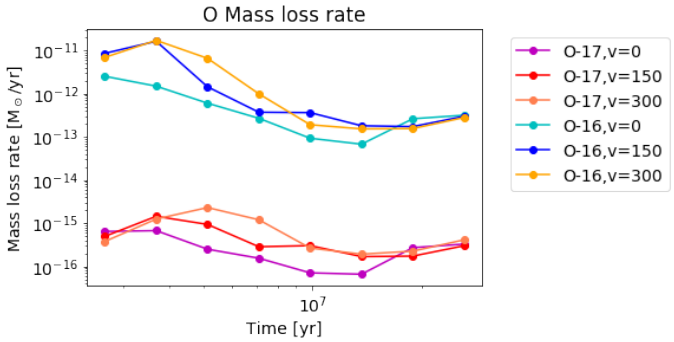

Fig. 5.4 O mass-loss rate for simulations 3,4

11 References

References

[Abbott-Conti] Abbott, D. C. 1987. Conti, P.S, Wolf-Rayet Stars. Annual Reviews Astronomy and Astrophysics. Vol(25:113-50)

[Abbott] Abbott, D. C, Bieging, J. H., Churchwell, E., Torres, A. V. 1986. Ap. J. 303: 239

[Limongi-Chieffi] Limongi, M.,Chieffi, A.,2018,Presupernova evolution and explosive nucleosynthesis of rotating massive stars in the metallicity range -3 $\leq$ [Fe/H] $\leq$ 0, Ap. JS.

[Ritter et al.] Ritter C.,Côté B., Herwig F.,Navarro J.F.,Fryer C.L.,2017,SYGMA (Stellar Yields for Galactic Modeling Applications), The Astrophysical Journal Supplement Series, Volume 237, Issue 2, article id. 42, 14 pp.

- -